MOLEKUL
eISSN: 2503-0310

Articles
https://doi.org/10.20884/1.jm.2023.18.3.9126

Glycine-modulated Zirconium Perylene-based Metal-Organic Framework for Rhodamin B Photocatalytic Degradation

Agustino Zulys[1*], Mella Defania[1], Jarnuzi Gunlazuardi[1], Adawiah[2]

[1]Department of Chemistry, Faculty of Mathematics and Natural Sciences, University of Indonesia, Depok 16424, Jawa Barat, Indonesia
[2]Integrated Laboratory Centre, Faculty of Science and Technology UIN Syarif Hidayatullah Jakarta Tangerang Selatan 15412, Indonesia

*Corresponding author email: zulys@ui.ac.id

Received July 09, 2023; **Accepted** September 11, 2023; **Available online** November 20, 2023

ABSTRACT. Photocatalysis employing Metal-Organic Framework (MOF) material may degrade Rhodamin B pollutant. MOF photocatalytic activity can be adjusted by altering the ligands, metal ions, and modulators. This research aims to synthesize glycine-modulated zirconium perylene-based metal organic framework (Zr-PTCA-Gly) for Rhodamin B photocatalytic degradation under visible light irradiation. The activated Zr-PTCA-Gly 1:10 exhibits good catalytic activity to degrade Rhodamine B with a 95.8% degradation efficiency.

Keywords : Glycine, metal organic framework, perylene, photocatalyst, Rhodamin B.

INTRODUCTION

Dyes are widely employed in a variety of industries, including food processing, cosmetics, plastics, paper, and textiles. Some dyes have good water persistence but are often poisonous or carcinogenic, causing harm to ecosystems and human health (Decoste et al., 2014). As a result, dye waste must be processed before it is released into the environment.

Several technologies have been widely employed to degrade dye pollutants like advance oxidation processes (AOPs), including Fenton reactions (Nidheesh et al., 2013), photocatalysis (Adawiah et al., 2022; Zulys et al., 2022; Saridewi et la., 2022), ozonation (Hassan et al., 2017), sonolysis and its combinations (Joseph & Taufiq Yap, 2017). Photocatalysis is regarded as an opportune way for treating organic dye waste because it is a non-toxic and low-cost treatment technology. It transforms organic dye pollutants into less harmful molecules, carbon dioxide, and water, and it turns photons from solar energy into chemical energy (Jin et al., 2018; Li et al., 2020).

Metal organic framework (MOF) is a group of porous materials made from metals and organic ligands which form a framework (Yuan et al., 2018). MOFs feature benefits over other types of semiconductor materials like metal oxide TiO_2 and ZnO as photocatalysts that provide high degradation efficiency only in ultraviolet area, such as valence and conduction band gaps that can be altered by selecting the proper metals and organic ligands (Shen et al., 2015). Building visible light-harvesting MOFs with photoactive metal ions or organic linkers improves photocatalytic activity. Organic linkers with numerous π-conjugated interactions have great potential as photosensitizers and can narrow the semiconductor band gap.

Perylene-3,4,9,10-tetracarboxylic acid (PTCA) is an aromatic compound having numerous π-conjugated bonds and four carboxylate groups. It could be used as an organic linker in the synthesis of visible light-responsive MOF-based photocatalysts. Batubara et al. (2019) reported a 2,6-naphthalene dicarboxylate (NDC)-based La-MOF with a band gap energy (Eg) of 3.1 eV. Then, Zulys et al. (2021) produced La-MOFs based on the organic linker 3,4,9,10-perylene tetracarboxylic dianhydride (PTCDA) with a band gap energy (Eg) of 2.21 eV. It implies that the perylene-based organic linker produced MOFs with the smaller energy band gap than NDC.

Photoactive metals, on the other hand, boost the photocatalytic activity of MOFs, such as zirconium (Zr) metal in its oxide state, which is photoactive and responsive to visible light. Haryanto et al., (2021) discovered that UiO-66 has higher photocatalytic activity than Cu-BDC for the breakdown of methyl orange (MO) under visible and UV light. Because zirconium is a strong Lewis acid with a high affinity for oxygen, the resulting MOF will be stable due to the stable Zr-O bonds (Marshall et al., 2016). Ahmadijokani et al., (2022) observed that the zirconium metal-based MOF UiO-66 is very

appealing for wastewater treatment applications. The fascinating properties of UiO-66, such as high thermal stability, superior chemical resistance to several solvents, including benzene, acetone, alcohols, dimethylformamide, acidic and basic solution, excellent chemical stability against various conditions, such as air, water, and chloroform, and exceptional resistance to high external pressure, are primarily due to the Zr-O solid bond and high coordination number between the Zr clusters and organic ligands. Taddei et al., (2019) also discovered that the zirconium-based MOF UiO-66 degraded Rhodamin B.

Furthermore, adding a modulator such as glycine, proline, phenylalanine, or benzoic acid to the MOF can improve its catalytic activity (Chambers et al., 2017; Gutov et al., 2016; Hasan, 2015). MOFs with high crystallinity, small particle sizes, and high porosity can be produced by amino acid modulation, which is desirable in dye catalytic photodegradation. Gutov et al., (2016) created a high porosity MOF by synthesizing amino acid-modified Zr-MOF. They reduced crystal defects, which were the primary causes of recombination throughout the photocatalysis process. Lin et al., (2018) found that UiO-66 derivatives made with amine (NH_2)-containing ligan greatly increased acid dye adsorption capacity and photocatalytic activity when exposed to visible light. Then, Dong et al., (2017) found that using glycine as a modulator enhances the activity and catalytic stability of MOF MIL-53 (Fe) because carboxylate and amine functional groups can bind metal ions. Adawiah et al., (2022) also reported that glycine-modified Cr-PTC-Gly removes methylene blue via adsorption and photocatalytic mechanisms that are greater than Cr-PTC.

The porosity and surface area of MOF are critical in its use. However, these pores can be filled with solvents with a high boiling point, such as dimethylformamide (DMF), diethyl formamide (DEF), or dimethyl sulfoxide (DMSO), which are commonly utilized in the synthesis of MOFs (Bae et al., 2018). Therefore, the solvent-exchange approach was used to release trapped solvent molecules in the MOF system.

Based on literature studies, the modulation of Zr-MOF using glycine and activated that MOF by solvent-exchange method to enhance its photocatalytic activity under visible light irradiation has never been carried out. As a result, this work aims to fabricate zirconium metal-based MOF (Zr-MOF) with PTCA ligands and modulated by glycine amino acids to obtain photoactive MOF for rhodamin B degradation under visible light irradiation. The synthesized Zr-PTC-Gly was then activated using the solvent-exchange method to assess the influence of activation on the structure, morphology, and photocatalytic activity of MOF in the degradation of rhodamine B.

EXPERIMENTAL SECTION

Materials

The materials used in this study were $ZrCl_4$ (Merck), Perylene-3,4,9,10 tetracarboxylic dianhydride (Sigma-Aldrich), Glycine (Sigma-Aldrich), NaOH (Merck), Na_2SO_4 (Merck), HCl (Merck), N,N-dimethylformamide (Merck), Dichloromethane (DCM), ethanol (Merck), methanol (Merck), distilled water, Rhodamin B (Merck).

Preparation of Perylene-3,4,9,10-Tetracarboxylic Acid (PTCA)

Perylene-3,4,9,10-tetracarboxylic dianhydride (PTCDA) (0.2 g, 0.5 mmol) was dissolved in 20 mL NaOH 5% and magnetically stirred for 1 h at 70 °C to obtain a yellow suspension. Furthermore, HCl 2M was added until the pH was 3-4. Then, the red precipitate was filtered and washed with distilled water and ethanol until it was neutral pH. The final red precipitate was dried at room temperature overnight, and analyzed using FTIR.

Fabrication of Zr-PTCA-Gly

A concentrated HCl (0.05 mL), 5 mL DMF, $ZrCl_4$ anhydrous (0.1398 g, 0.6 mmol, 1 eq), and glycine solution (0.2252 g, 3.0 mmol, 5 eq and 0.4504, 6.0 mmol, 10 eq) were put into the 50 mL pyrex vials. Then, the mixture was sonicated for 5 min. After that, PTCA (0.6 mmol, 0.2569 g, 1 eq in 5 mL DMF) was added to the mixture. Furthermore, the mixture was sonicated for 5 min and heated at 120 °C for 24 h. The obtained glycine-modulated Zr-MOF (Zr-PTC-Gly) was filtrated and washed using 10 mL of DMF and 10 mL of water-methanol (9:1 v/v). Furthermore, Zr-PTC-Gly was dried at 70 °C overnight. Finally, Zr-PTC-Gly was activated with dichloromethane and dried at 120 °C for 24 hours. The final product was designed as Zr-PTC-Gly-(1:5) and Zr-PTC-Gly (1:10) for the 5 eq and 10 eq glycine in 2 mL of distilled water, respectively.

Zr-PTCA-Gly Characterization

The obtained Zr-PTCA-Gly MOF was characterized using FTIR Prestige-21 Shimadzu with KBr pellet for the background measurement and wavenumber range of 4000–400 cm^{-1}. The PXRD Shimadzu XRD 7000 Maxima-X (Cu-Kα radiation (λ = 1.5418 Å) with the scan rate of 2º min^{-1} at room temperature on the 2θ angle of 2º–80º. The UV-Vis Spectrophotometer Agilent Carry 60 with $BaSO_4$ as a reference at 200-800 nm. The FESEM-EDS analysis using FEI Quanta 650. The Brunauer-Emmett-Teller (BET) method on a Micromeritics TriStar II Surface Area and Porosity. Thermogravimetric analysis (TGA-DTA) using TGA Q50 V20.13 Build 39 at the heating rate of 10 ºC min^{-1} under an air atmosphere. As well as multi-pulse amperometry (MPA) analysis using fluorine-doped Tin Oxide glass (FTO glass) working electrodes, Ag/AgCl comparison electrodes, and Pt supporting electrodes, with Na_2SO_4 0.1 M electrolyte.

Zr-PTCA-Gly Photocatalytic Activity Test

Zr-PTCA-Gly MOF (30, 45 and 50 mg) was dispersed into 50 mL of Rhodamin B solution (10 ppm). Then, the mixture was stirred at 300 rpm at room temperature and left for 30 minutes in dark conditions to achieve adsorption-desorption equilibrium. Furthermore, the suspension was irradiated with a 250-watt mercury lamp as a visible light source for 2 hrs. Then, 2 mL of suspension was taken and centrifuged. The RhB absorbance was measured using a UV-Vis spectrophotometer at 555 nm. The degradation efficiency and degradation capacity of RhB was calculated using equation 1.

$$DE\ (\%) = \frac{(Ao-At)}{Ao} \times 100\% \quad (1)$$

$$DC\ (mg/g) = DE \times Co \times \frac{V}{m} \quad (2)$$

Where DE is degradation efficiency (%), DC is degaration capacity (mg/g), Ao and At are the initial absorbance and absorbance at a given reaction time, Co is the initial RhB concentration, V is RhB volume (L) and m is MOF dosage (g).

RESULT AND DISCUSSION

FTIR spectrum showed a very sharp absorption peak at 1026 cm^{-1}, which indicates a CO-O-CO stretching of the PTCDA (**Figure 1**). The shift peak from 1776 cm^{-1} to 1700 cm^{-1} confirmed a difference in the stretching vibration of C=O between PTCDA and PTCA. The absorption peak shift to a lower wavenumber indicates a change in the bond length or interaction with different side atoms of the carboxyl group in PTCDA and PTCA. In addition, in the PTCA spectrum, a widening absorption peak at 2998 cm^{-1} indicates vibration of the O-H stretching of the carboxylic acid group.

Figure 2 demonstrates a shift of the C=O vibrational absorption band in PTCA from 1693 cm^{-1} to 1776 cm^{-1} (Zr-PTCA) and 1694 cm^{-1} (Zr-PTCA-Gly). It implies that a new bond between zirconium metal and ligands was formed. In addition, a band at 1026 cm^{-1} is attributed to the interaction of the COO- with Zr. A band at 3550 cm^{-1} revealed N-H stretching vibration in Zr-PTC-Gly before activation. However, in activated Zr-PTC-Gly, the probability of its peak is covered by the O-H stretching denoted by the presence of a band at 3000-3550 cm^{-1}, suggesting stretching -OH stretching of H_2O. It is confirmed by the peak at 3200-3550 cm^{-1} in activated Zr-PTCA-Gly, which is wider than the non-activated Zr-PTC-Gly. Due to DMF, solvents that may be trapped in the Zr-PTC-Gly pore or coordinated bound to the framework and cover the active site of the MOF are no longer present.

Figure 3 shows that the difference in the PTCA, Zr-PTCA and Zr-PTCA-Gly XRD diffraction. It illustrates that Zr-PTCA-Gly is already formed. The peak at 2θ = 12.35° and 27.33° in PTCA is still present on non-modulated Zr-MOF with a slight shift. It is estimated that the MOF washing process has not been clean. The Zr-PTCA, Zr-PTCA-Gly (1:5) and Zr-PTCA-Gly (1:10) XRD diffraction accomplished not vary significantly, but there was a slight shift (**Figure 3a**). New peaks appeared on Zr-PTCA-Gly (1:5) and Zr-PTCA-Gly (1:10), indicating a new bond formed between the glycine modulator and Zr-PTCA. Zr-PTCA-Gly (1:10) XRD diffraction reveals peaks at 2θ = 7.15°; 13.97°; 15.59°; 19.01°; 22.25°; 24.20°; 25.58°; 27.21°; 28.83°; 29.56°; 35.08°; 41.80° (**Figure 3b**). There were no significant differences in diffraction patterns between Zr-PTCA-Gly (1:10) before and after activation, indicating that the activation treatment did not change the structure of the Zr-PTCA-Gly (1:10).

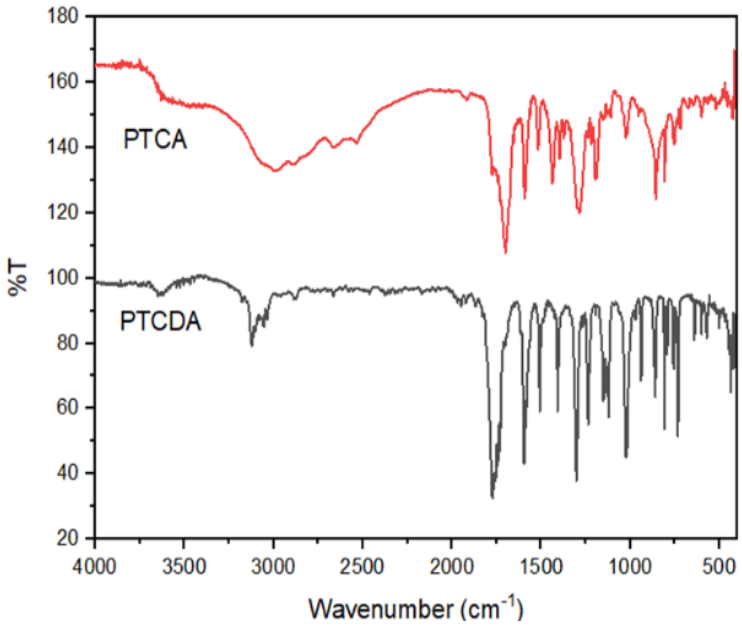

Figure 1. FTIR spectrum of PTCDA and PTCA

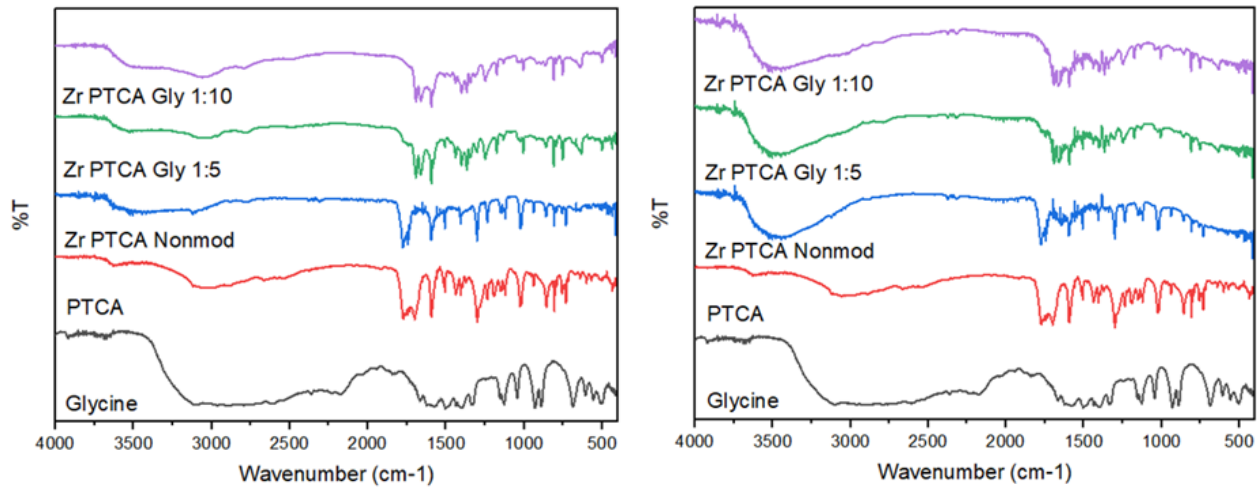

Figure 2. FTIR spectrum of (**a**) non-activated material and (**b**) activated material

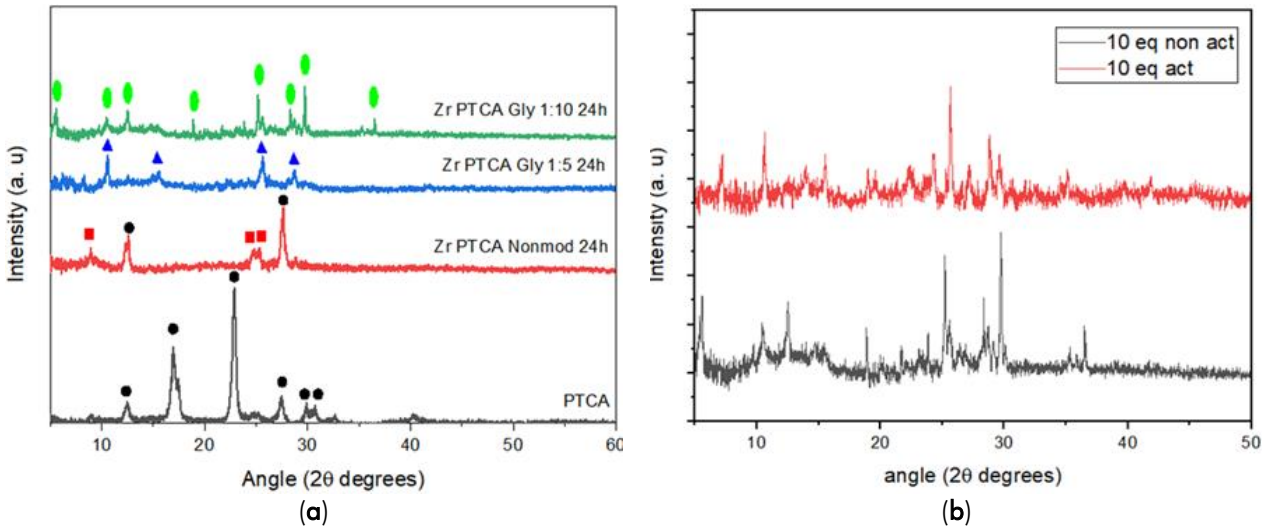

Figure 3. XRD diffraction patter of (**a**) PTCA, Zr-PTCA, Zr-PTCA-Gly 1:5 and Zr-PTCA-Gly 1:10; (**b**) Zr-PTCA-Gly 1:10 activated and non-activated

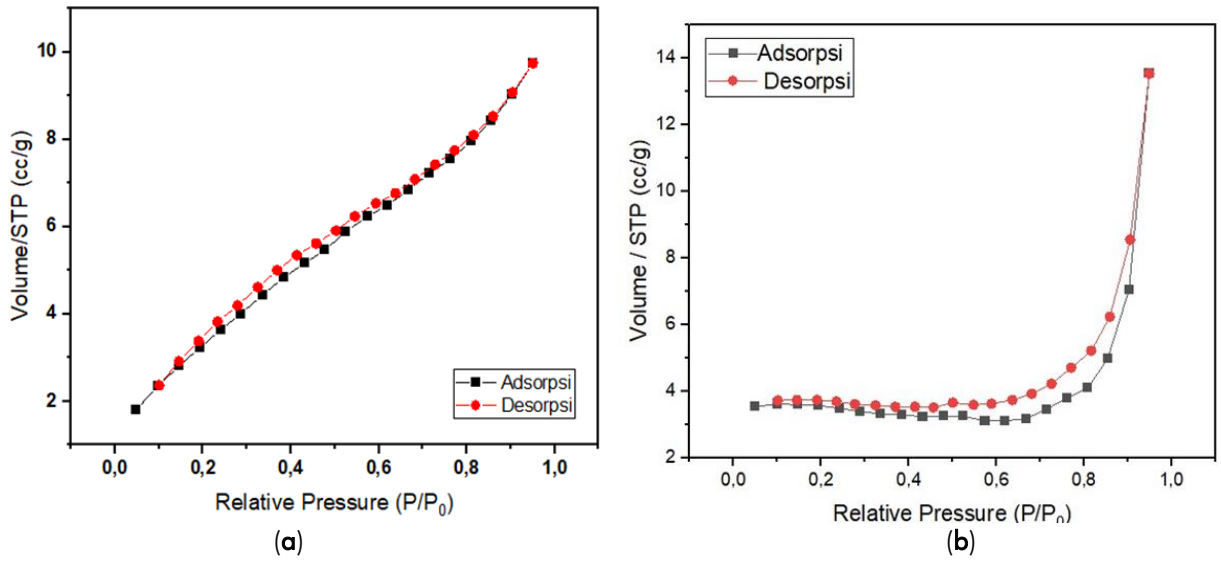

Figure 4. Adsorption-desorption isotherm graph of (**a**) non-activated Zr-PTCA-Gly 1:10; and (**b**) activated Zr-PTCA-Gly 1:10

Figure 4 showed that the non-activated Zr-PTCA-Gly (1:10) follows the pattern of the type IV adsorption isotherm curve shape. Type IV adsorption isotherms indicate that the material is mesoporous. There is a hysteresis or gap between the adsorption and desorption lines. However, the type of isotherm of activated Zr-PTCA-Gly (1:10) is unknown because the data needs to be representative.

The largest pore size distribution for non-activated and activated Zr-PTCA-Gly (1:10) about 2-4 nm. The obtained surface area is 13.874 m^2/g and 1.568 m^2/g for non-activated and activated Zr-PTCA-Gly (1:10). Compared to UiO-66, a Zirconium metal-based MOF with H_2BDC ligands, synthesized Zr-MOF in this study has a relatively very small surface area. It is estimated that due to the impurity of the sample and the formation of MOF crystal defect. The activated Zr-PTCA-Gly-10 has a smaller surface area than non-activated Zr-MOF. It may occur if the degassing temperature of the material used during the measurement is too high. In dye photocatalysis degradation, the material's surface area and pore size play an important role (Kudo and Miseki, 2009). It is related to the porosity and surface area function both in the adsorption mechanism and in the photocatalysis process. The greater the surface area, the more active sites play a role in photocatalysis. Therefore, a large surface area can increase photocatalytic activity in dye degradation.

The thermogravimetric analysis (TGA) shows an initial weight loss in the 50-160 °C temperature range of 4.796%, indicating the break of the bond with H_2O and the possible presence of DMF solvents (**Figure 5**). Furthermore, it lost weight in the range of 160-275 °C, as much as 11.56%. This decrease occurs due to the release of the amino acid glycine, which has a boiling point of 240.9 °C. In the temperature range of 275-450 °C, there is a weight loss of 20.24%. Then the temperature range of 450-500 °C loses weight of about 8.423% is suspected to be the decomposed temperature of the MOF. The TGA-DTG chart above shows that the unactivated Zr-PTCA-Gly (1:10 24h) is thermally stable at a temperature range of 200-300 °C.

Figure 6 revealed that the morphology of Zr-MOF, both modulated and unmodulated, resembles a rod with a size of about 1 micron for non-modulated and 5 microns for modulated. The morphology of unmodulated Zr-MOF is less consistent than the modulated Zr-MOF (Zr-PTCA-Gly-10). Using a modulator can improve the morphology of the Zr-PTCA. Zr-PTCA contains the most elements, C (62.1%), followed by Zr (21.8%), then O (16.1%). Meanwhile, Zr-PTCA-Gly (1:10 24h) contains the most elements, namely C (74.2%), Zr (14.2%), O (11.6%), and N (0.0%), which indicates that the amino acid glycine binds to Zr-PTCA. The percent weight (%wt) of the Nitrogen (N) is small because it is likely that measurements are only carried out on one side where there is little modulation, so it does not represent the full distribution. However, the mapping analysis showed that the N element is actually contained in the modulated Zr-PTC structure (**Figure 6**). The lowering of Zr and O components indicates the possibility of missing ligand defects and missing cluster defects due to modulation.

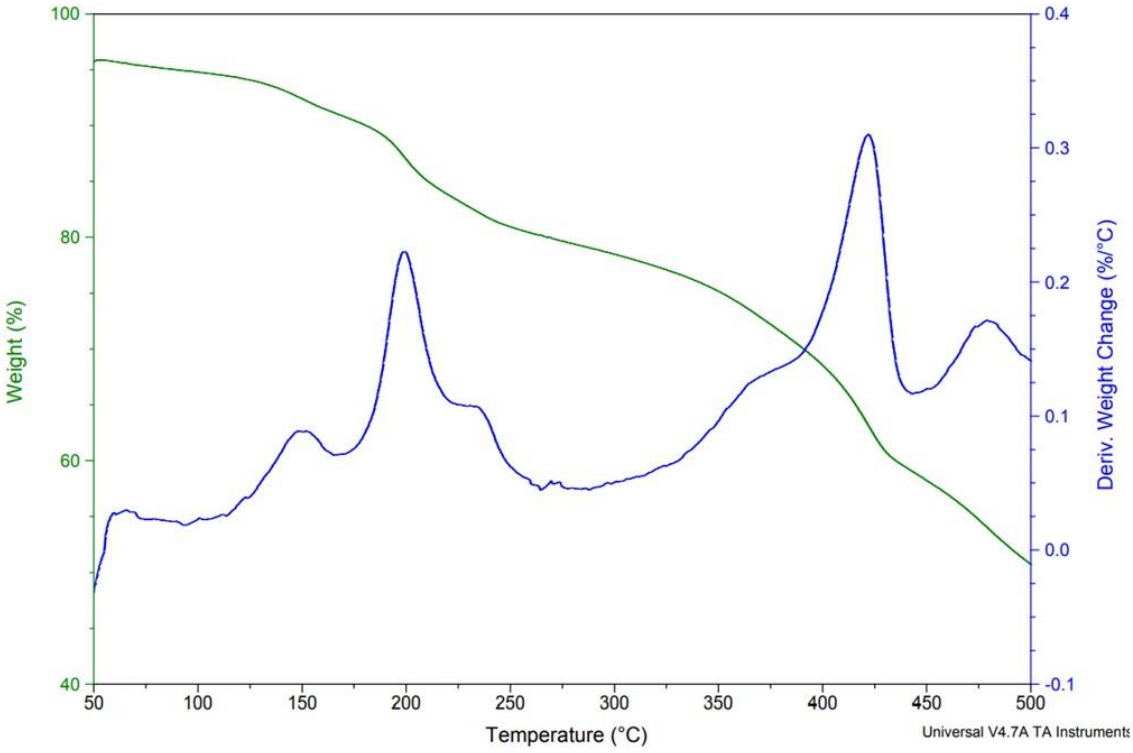

Figure 5. TGA curve of non-activated Zr-PTCA-Gly 1:10

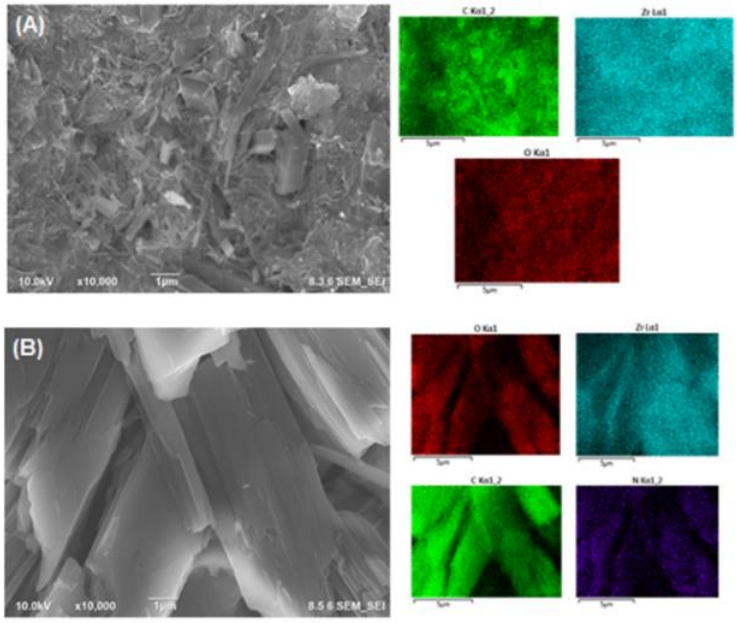

Figure 6. FESEM-EDS images dan element mapping (A) non modulated-Zr MOF and (B) glycine modulated-Zr-MOF

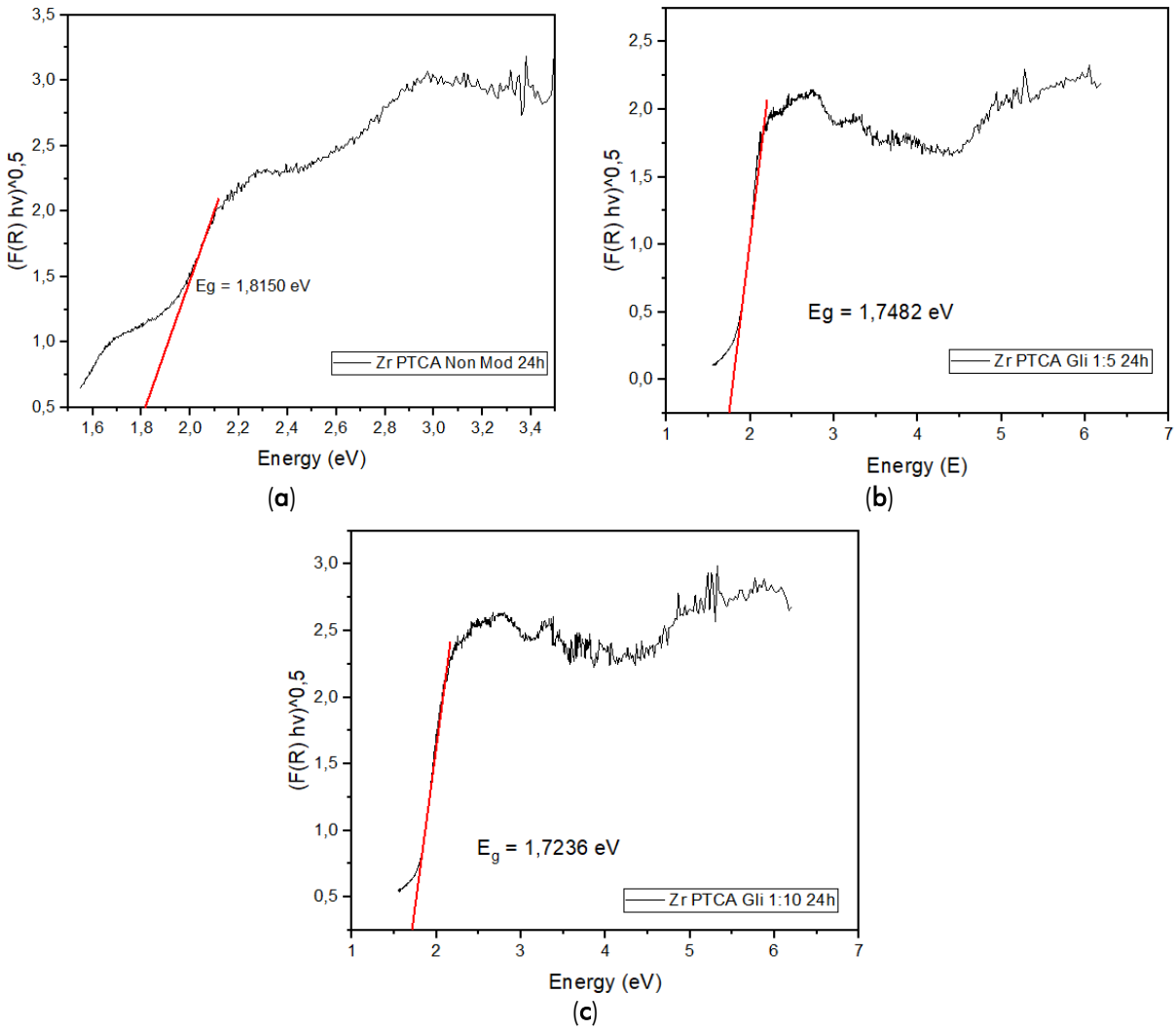

Figure 7. Diagram of bandgap energy (Eg) of activated Zr-MOF (**a**) non-modulated Zr-MOF; (**b**) Zr-PTCA-Gly 1:5; and (**c**) Zr-PTCA-Gly 1:10

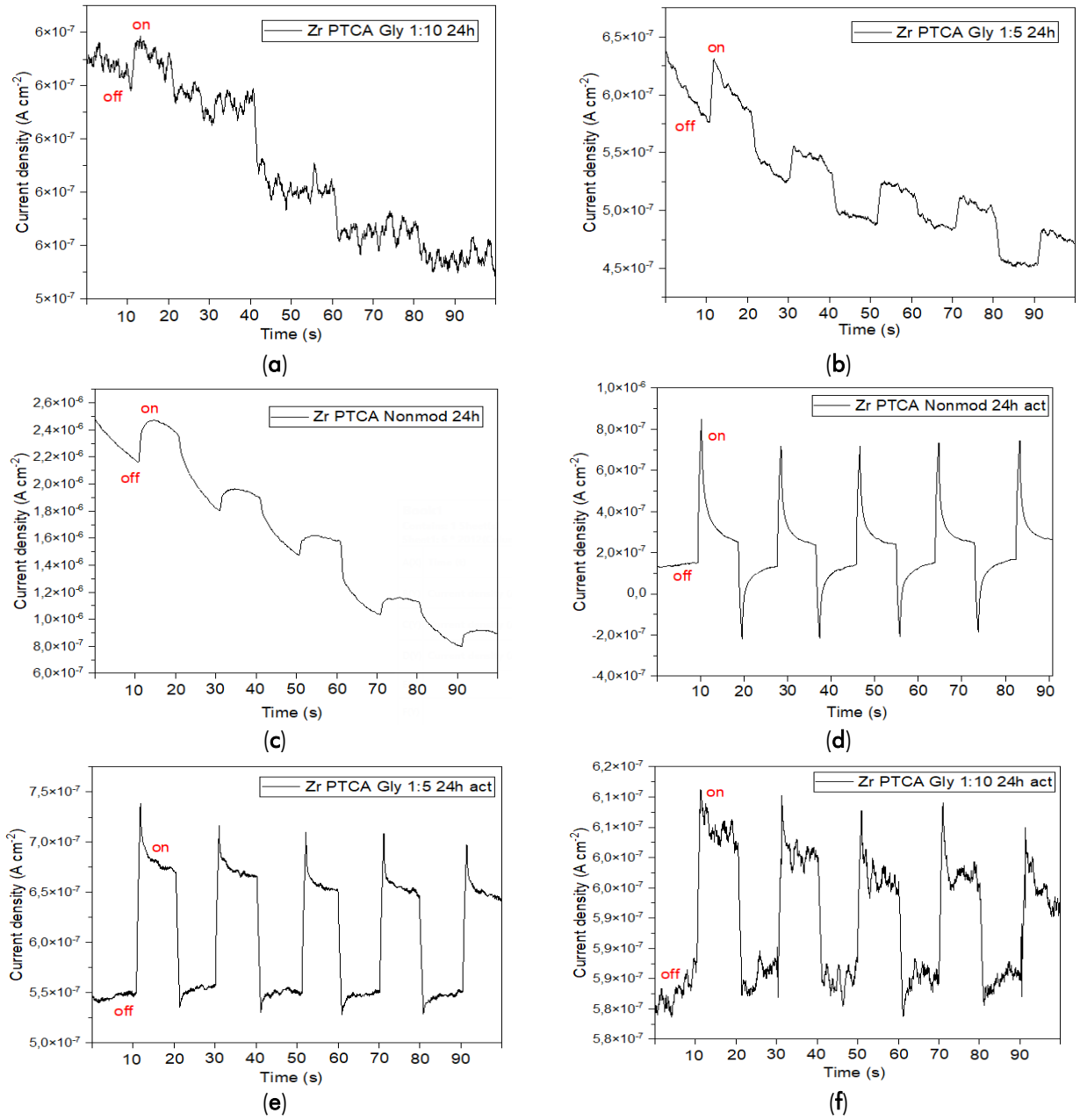

Figure 8. Multi Pulse Amperometry graph of (**a-c**) non-activated Zr-MOF; and (**d-f**) activated Zr-MOF

UV DRS analysis data was employed to measure the bandgap energy of activated Zr-MOF using Kubelka Munk-Tauc Plot equation (Makula et al., 2018). Activated Zr-MOF provide a lowering in band gap energy that is proportional to the addition of the modulator mole ratio, namely 1.8150 eV (Zr-PTCA), 1.7428 eV (Zr-PTCA-Gly (1:5) and 1.7236 eV (Zr-PTCA-Gly (1:10) (**Figure 7**). The three activated Zr-MOF produced have a relatively small band gap energy. It implies that activated Zr-MOF has the potential to evolve a visible light-responsive photocatalyst material. Photoresponsive materials create an electric current when exposed to light in the Multi Pulse Amperometry (MPA) characterization (**Figure 8**). Visible light is used in this study. When the energy of the light is equivalent to the band gap energy of the material, leading electrons and holes to form as a result of electron excitation from the valence band to the conduction band (Saravanan et al., 2017). The electron-hole pair can be kept in place to carry out the redox process. The electrons will then flow to the system's electrodes, generating a current that can be measured using the sensor. Assume that all pairs of electrons and holes in the material immediately recombine following stimulation. In that instance, there is no flow of electrons in the system, and the electric current cannot be read. The current generated in this system is determined by the efficiency of generating electron and hole pairs in the semiconductor.

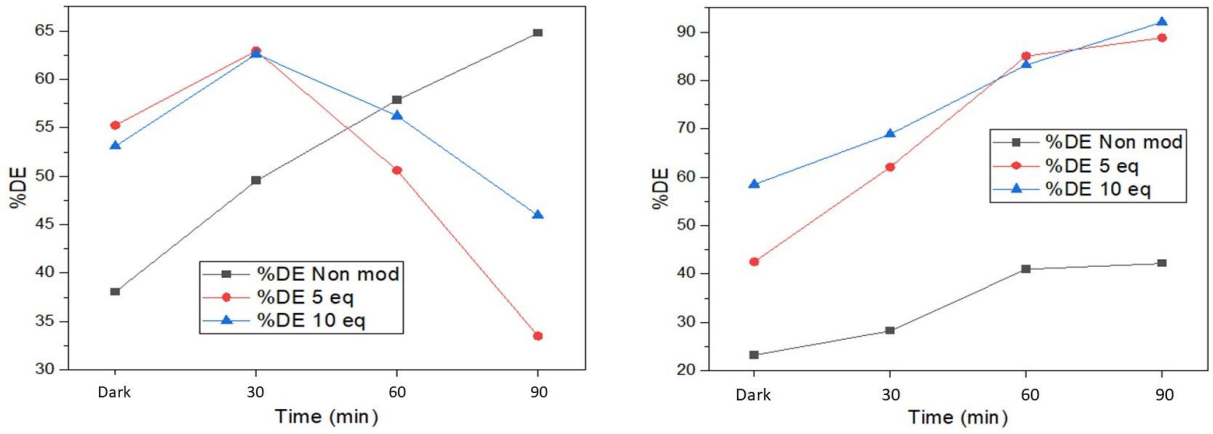

Figure 9. Rhodamin B degradation efficiency of (**a**) non-activated materials and activated materials

Figure 9a shows that the modulated Zr-MOF exhibited no photocatalytic activity. The fluctuating degradation efficiency confirmed it. On the other hand, the photocatalytic activity of non-modulated Zr-MOF (Zr-PTCA) is better than modulated Zr-MOF (Zr-PTC-Gly) with degradation efficiency of 64.78% and 42.16%, respectively (**Figure 9a**). It is because non-activated MOF tends to be less stable when exposed to light, so it undergoes desorption, as shown in **Figure 8**, which tends to decrease its current density. Meanwhile, after activation, the modulated Zr-MOF tended to have a greater degradation than the non-modulated Zr-MOF. Zr-PTC-Gly (1:5) and Zr-PTC-Gly (1:10) achieved 88% and 92% degradation efficiency within 90 minutes. Due to before activation, MOF has more NH_2 groups from DMF than after activation. This group may affect the photocatalytic process and lower the band gap energy, increasing the degradation compared to after activation.

The activated Zr-PTCA-Gly 1:5 exhibited the highest photocatalytic activity with increasing degradation efficiency of 45% after 90 min of light irradiation (**Figure 9**). It was due to the higher adsorption of RhB molecules on activated Zr-PTCA-Gly 1:10 than Zr-PTCA-Gly 1:5, which was confirmed under dark conditions. The high RhB molecules adsorbed on the surface of Zr-PTCA-Gly 1:10 lead to a decrease in photocatalytic activity by inhibiting the light hitting the surface of Zr-PTCA-Gly 1:10 and reducing the electron excitation process on the surface of Zr-PTCA-Gly 1:10, which results in a decrease in the formation of radical species that play an essential role in the photocatalytic degradation of RhB. However, in this work, activated Zr-PTCA-Gly 1:10 was employed for the following analysis because it exhibited the highest degradation efficiency of RhB both via adsorption and photocatalytic mechanism.

Figure 10 demonstrates that the Zr-PTC-Gly-10 MOF gave a percentage RhB degradation efficiency of 95.8%, 94.5%, and 94% or a degradation capacity of 15.96 mg/g, 7.87 mg/g, and 7.83 mg/g for MOF doses of 30 mg, 45 mg, and 60 mg, respectively. Zr-PTCA-Gly 1:10 dosage of 30 mg exhibited the highest photocatalytic degradation efficiency as it obtained the highest RhB degradation via the photocatalytic degradation mechanism, which was 37%. At MOF amounts of 45 and 60 mg, RhB degradation was mainly influenced by the adsorption ability of MOF.

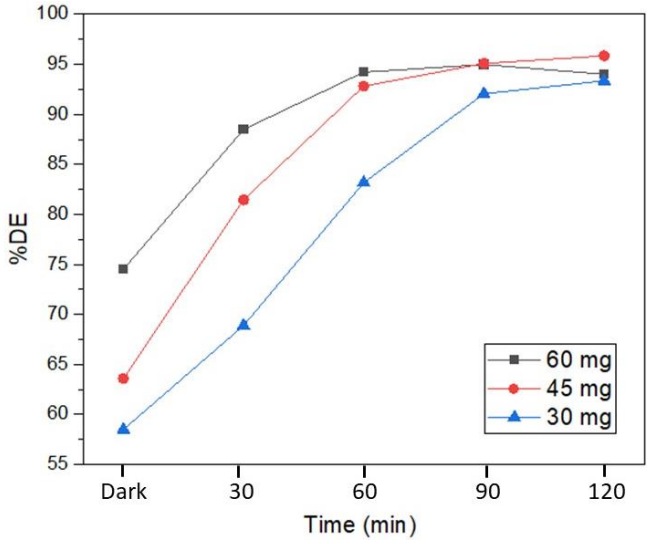

Figure 10. RhB degradation efficiency in various dosage of activated Zr-PTC-Gly (1:10)

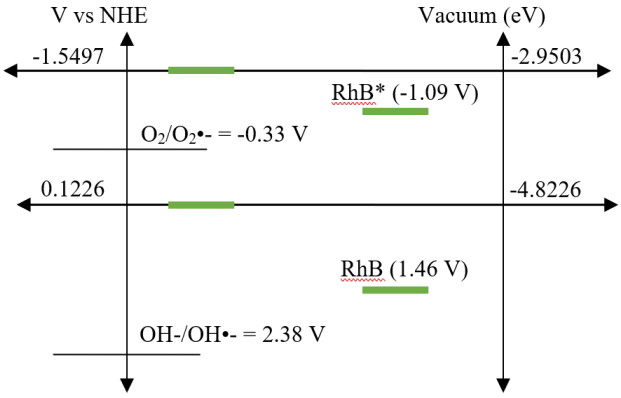

Figure 11. Energy diagram of activated Zr PTCA Gly 1:10

The higher the dose of MOF added into the RhB solution, the more MOF particles adsorbed RhB. On the other hand, there was a decline in RhB degradation efficiency by 60 mg MOF at 120 minutes of irradiation. The increase in MOF dosage caused the MOF particles to agglomerate so that the MOF active sites were close together and inhibited the degradation of RhB.

Photocatalysis must have a band gap energy that approximates the required energy level for the desired redox reaction. The redox potential must be converted to Normal Hydrogen Electrode (NHE) before it is employed to estimate the energy diagram. The voltammetry cyclic analysis outcomes demonstrate the activated Zr PTCA Gly 1:10 energy diagram (**Figure 11**). **Figure 11** exhibited that the redox species that play a role in degradation are $O_2/•O_2^-$ and $OH^-/•OH$. The reduction potential of $O_2/•O_2^-$ is -0.33V, and the oxidation potential of $OH^-/•OH$ is 2.38V. These potential values must be met to generate radical species and then react to dye to obtain degraded products. Therefore, the oxidation potential of Zr-MOF should be more positive than 2.38 V, and the reduction potential of Zr-MOF should be more negative than -0.33 V. **Figure 11** demonstrates that the OH-/OH• reaction cannot occur because the Zr-MOF oxidation potential (HOMO) value is not more positive than the $OH^-/OH•$ potential. Hence, the energy is insufficient to oxidize OH^- to OH•. Therefore, the degradation process is estimated to affect superoxide free radicals ($•O_2^-$) originating from the $O_2/•O_2^-$ reduction reaction because the reduction potential (LUMO) of Zr-MOF is more negative than the reduction potential of $O_2/•O_2^-$. The degradation of Rhodamine B dye by Zr-MOF affects excited electrons, which produce a radical source originating from $O_2 + e^- \rightarrow •O^{2-}$ which will then react with H^+ ions to form HOO• and finally create OH• radicals for Rhodamine degradation B.

CONCLUSION

The solvothermal method successfully synthesized the glycine-modulated Zr-MOF (Zr-PTC-Gly) with lower band gap energy than Zr-PTC. The activation treatment eliminated the trapped solvent molecule, preserving the MOF morphology and structure. The activation treatment enhances the glycine-modulated Zr-MOF (Zr-PTC-Glyy-10) photocatalytic activity in RhB degradation, where the optimum MOF dosage is 45 mg for 90 min.

ACKNOWLEDGEMENT

The authors would like to acknowledge the Directorate of Research and Community Engagements, Universitas Indonesia, to support this research through Hibah Riset FMIPA UI with contract number NKB-003/UN2.F3/HKP.05.00/2021.

REFERENCES

Adawiah, A., Fitria, R. N., Saridewi, N., Oktavia, W., Azhar, F. M., Gunawan, M. S., & Komala, S. (2022). Synthesis glycine-modulated metal organic framework cr-ptc-gly for synergetic methylene blue adsorption and photodegradation under visible light irradiation. *Molekul*, *17*(3), 373 – 382. https://doi.org/10.20884/1.jm.2022.17.3.6126.

Ahmadijokani, F., Molavi, H., Rezakazemi, M., Tajahmadi, S., Bahi, A., Ko, F., Aminabhavi, T. M., Li, J. R., & Arjmand, M. (2022). UiO-66 metal–organic frameworks in water treatment: A critical review. *Progress in Materials Science*, *125*, 100904. https://doi.org/10.1016/j.pmatsci.2021.100904.

Bae, J., Lee E., & Jeong, N. (2018). Metal coordination and metal activation abilities of commonly unreactive chloromethanes toward metal-organic frameworks. *Chemical Communication*, *54*, 6458 – 6471. DOI: 10.1039/c8cc02348d

Batubara, N. H., & Zulys, A. (2019). Synthesis, structural, spectroscopic, and morphology of metal-organic frameworks based on La (III) and ligand 2,6-napthalenedicarboxylic acid (La-MOFs) for hydrogen production. *IOP Conf. Ser.: Mater. Sci. Eng. 546,* 042005. doi:10.1088/1757-899X/546/4/042005.

Chambers, M. B., Wang, X., Ellezam, L., Ersen, O., Fontecave, M., Sanchez, C., & Mellot-

Draznieks, C. (2017). Maximizing the Photocatalytic activity of metal-organic frameworks with aminated-functionalized linkers: substoichiometric effects in MIL-125-NH_2. *Journal of the American Chemical Society*, *139*(24), 8222–8228. https://doi.org/10.1021/jacs.7b02186

DeCoste, J. B., & Peterson, G. W. (2014). Metal−organic frameworks for air purification of toxic chemicals. *Chem. Rev.*, *114*(11), 5695–5727. https://doi.org/10.1021/cr4006473.

Dong, W., Yang, L., & Huang, Y. (2017). Talanta glycine post-synthetic modification of MIL-53 (Fe) metal-organic framework with enhanced and stable peroxidase-like activity for sensitive glucose biosensing. *Talanta*, *167*(November 2016), 359–366. https://doi.org/10.1016/j.talanta. 2017.02.039

Gutov, O. V., Molina, S., Escudero-Adán, E. C., & Shafir, A. (2016). Modulation by amino acids: toward superior control in the synthesis of zirconium metal–organic frameworks. *Chemistry-A European Journal*, *22*(38), 13582–13587. https://doi.org/10.1002/chem. 201600898

Haryanto, A., Mukaromah, L., Permana, Y., & Patah, A. (2021). Photocatalytic activity of CuBDC and UiO-66 MOFs for methyl orange degradation. *Journal of Chemical Technology and Metallurgy*, *56*(4), 791-795.

Hasan, M. R. (2015). Pengaruh penambahan modulator asam asetat pada sintesis metal organic framework tipe HKUST-1 (Effect of adding acetic acid modulator on the synthesis of metal organic framework type HKUST-1). Institut Teknologi Sepuluh Nopember Surabaya.

Hassaan, M. A., Nemr, A. E., & Madkour, F. F. (2017). Advanced oxidation processes of Mordant Violet 40 dye in freshwater and seawater. *The Egyptian Journal of Aquatic Research*, *43*(1), 1-9. https://doi.org/10.1016/j.ejar.2016.09. 004.

Jin, Z., Wang, L., Hu, Q., Zhang, L., Xu, S., Dong, X., Gao, X., Ma, R., Meng, X., & Xiao, F. (2018). Hydrophobic zeolite containing titania particles as wettability-selective catalyst for formaldehyde removal. *ACS Catalysis, 8*(6), 5250–5254. https://doi.org/10.1021/acscatal.8b00732.

Joseph, C. G., Taufiq-Yap, Y. H., & Krishnan, V. (2017). Ultrasonic assisted photolytic degradation of reactive black 5 (RB5) simulated wastewater. *ASEAN Journal of Chemical Engineering*, *17*(2):37-50. DOI:10.22146/ajche.49554.

Kudo, A., & Miseki, Y. (2009). Heterogeneous photocatalyst materials for water splitting. *Chemical Society Reviews*, *38*(1), 253–278. https://doi.org/10.1039/B800489G

Li, J., Cui, W., Chen, P., Dong, X., Chu, Y., Sheng, J., Zhang, Y., Wang, Z., & Dong, F. (2020). Unraveling the mechanism of binary channel reactions in photocatalytic formaldehyde decomposition for promoted mineralization. *Applied Catalysis B: Environmental*, *260*, 118-130. https://doi.org/10.1016/j.apcatb.2019. 118130.

Lin, K. A., Yang, H., & Hsu, F. K., (2018). Zr-metal organic framework and derivatives for adsorptive and photocatalytic removal of acid dyes. *Water Environ Res.*, *90*(2), 144-154. doi: 10.2175/106143017X15054988926604.

Makula, P., Pacia, M., Macyk, W. (2018). How to correctly determine the band gap energy of modified semiconductor photocatalysts based on UV−Vis spectra. *Journal of Physical Chemistry Letters*. *9*, 6814−6817. DOI: 10.1021/acs.jpclett. 8b02892.

Marshall, R. J., Hobday, C. L., Murphie, C. F., Griffin, S. L., Morrison, C. A., Moggach, S. A., & Forgan, R. S. (2016). Amino acids as highly efficient modulators for single crystals of zirconium and hafnium metal-organic frameworks. *Journal of Materials Chemistry A*, *4*, 6955-6963. doi: 10.1039/c5ta10401g

Nidheesh, P. V., Gandhimathi, R., & Ramesh, S. T. (2013). Degradation of dyes from aqueous solution by Fenton processes: a review. *Environmental Science and Pollution Research*, *20*, 2099–2132. https://doi.org/10.1007/s11356-012-1385-z.

Saravanan R., Gracia F., & Stephen A. (2017) Basic principles, mechanisms, and challenges of photocatalysis. In: Khan M., Pradhan D., Sohn Y. (eds) Nanocomposites for visible light-induced photocatalysis. *Springer Series on Polymer and Composite Materials*. Springer, Cham. doi:10.1007/978-3-319-62446-4-2

Saridewi, N., Komala, S., Zulys, A., Nurbayti, S., Tulhusna, L., & Adawiah, A. (2022). Synthesis of ZnO-Fe_3O_4 magnetic nanocomposites through sonochemical methods for methylene blue degradation. *Bulletin of Chemical Reaction Engineering & Catalysis*, *17*(3), 650-660. https://doi.org/10.9767/bcrec.17.3.15492.650-660.

Shen, L., Liang, R., Luo, M., Jing, F., & Wu, L. (2015). Electronic effects of ligand substitution on metal-organic framework photocatalysts: The case study of UiO-66. *Physical Chemistry, Chemical Physics: PCCP*, *17*(1), 117-121. doi:10.1039/C4CP04162C.

Taddei, M., Schukraft, G. M., Warwick, M. E. A., Tiana, D., McPherson, M. J., Jones, D. R., & Petit, C., (2019). Band gap modulation in zirconium-based metal-organic frameworks by defect engineering. *Journal of Materials Chemistry A*, *7*, 23781-23786

Yuan, S., Feng, L., Wang, K., Pang, J., Bosch, M., Lollar, C., & Zhou, H. C. (2018). Stable metal–organic frameworks: design, synthesis, and applications. *Advanced Materials*, *30*(37), 1–35. https://doi.org/10.1002/adma.201704303.

Zulys, A., Adawiah, A., & Nasruddin, N. (2022). Efficient degradation of methylene blue using La-PTC-HIna/$Ti_3C_2T_x$ MXene: adsorption and photocatalytic degradation. *Indonesian Journal of Chemistry*, *22*(5), 1195 – 1204. DOI: 10.22146/ ijc.71692.

Zulys, A., Adawiah, A., Gunlazuardi, J., & Yudhi, M. D. L. (2021). Light-Harvesting metal-organic frameworks (MOFs) La-PTC for photocatalytic dyes degradation. *Bulletin of Chemical Reaction Engineering & Catalysis*, *16*(1), 170-178. doi:10.9767/bcrec.16.1.10309.170-178.